Tissue repair modeling

Luis Almeida, Patrizia Bagnerini, Abderrahmane Habbal, Stéphane Noselli, Fanny Serman

▶ **To cite this version:**

Luis Almeida, Patrizia Bagnerini, Abderrahmane Habbal, Stéphane Noselli, Fanny Serman. Tissue repair modeling. Singularities in Nonlinear Evolution Phenomena and Applications, May 2008, Pisa, Italy. pp.27-46. ⟨hal-00480769⟩

HAL Id: hal-00480769

https://hal.science/hal-00480769v1

Submitted on 5 May 2010

HAL is a multi-disciplinary open access archive for the deposit and dissemination of scientific research documents, whether they are published or not. The documents may come from teaching and research institutions in France or abroad, or from public or private research centers.

L'archive ouverte pluridisciplinaire **HAL**, est destinée au dépôt et à la diffusion de documents scientifiques de niveau recherche, publiés ou non, émanant des établissements d'enseignement et de recherche français ou étrangers, des laboratoires publics ou privés.

HAL Authorization

Tissue repair modeling

Luís Almeida[1], Patrizia Bagnerini[2], Abderrahmane Habbal[1], Stéphane Noselli[3] and Fanny Serman[1,3]

[1] Laboratoire J.A. Dieudonné
Université de Nice
UMR 6621 CNRS
Parc Valrose
F-06108 NICE Cédex 02, FRANCE

[2] DIPTEM
Università degli Studi di Genova
P.le Kennedy-Pad D
16129 Genova, ITALY

[3] Institute of Developmental Biology & Cancer IBDC-Nice
Université de Nice
UMR 6543 CNRS
Parc Valrose
F-06108 NICE Cédex 02, FRANCE

This project was supported by the ACI NIM Momatsouti. Work in the SN laboratory is supported by CNRS, ANR, ARC, FRM, CEFIPRA.

1 Introduction

Tissue repair is an essential mechanism for assuring an organism's integrity and protection from external aggressions and it is active all through its life (from embryonic to adult stages). In embryos, this process is achieved through mechanisms that recall strongly those used for building the original tissue and yield perfect repair (regenerative repair in the sense of [2]). However, in many species (in particular for humans) adult wound healing generally involves different mechanisms and ends up generating a mass of fibrotic tissue commonly known as a scar. This fibrosis is not only aesthetically undesirable but has also serious clinical consequences, specially if we consider

that fibroctic healing is at the origin of many tissue malfunctions following a wide class of injuries from heart attacks to burns and cirrhosis (see [2] for a description of the biological and clinical issues related to wound healing and regeneration). A good understanding of regenerative healing mechanisms (such as embryonic wound healing and the closely related morphogenetic events like Dorsal Closure) and of how we can re-activate or reproduce them in adult setting is an important public health issue for the future.

Many recent works (see [2] and [6] for reviews) indicate that the switch between regenerative and fibroctic healing is probably linked to the inflammatory response and associated existence of a mature immune system. However, this shouldn't lead us to conclude that embryos always exhibit regenerative healing, while adults always display fibroctic healing. Things are not so simple since many species (amphibians, for instance) show remarkable regenerative capabilities even after they are adults. Moreover, small wounds in single layer adult epithelia may also heal using embryo-like mechanical processes (we will come back to this issue below) which gives another reason considering them.

An extra motivation for studying embryonic wound healing is that even if generally the main mechanisms are different from the adult case, it has been shown that there are many similarities concerning the genetic pathways involved in the two settings. Identifying them in the simpler setting of embryonic healing would help understanding their role in adult healing and, which brings us back to the first paragraph, the differences that we would detect would also give us clues as to how regenerative healing could be re-activated in an adult setting.

Wound healing in adult mammalian epithelia is classically divided into 3 stages:

a) Inflammation. (a stage that lasts for several hours after injury) The wound is rapidly plugged by a fibrin clot to prevent tissue and blood loss. There are many neutrophils and platelets inside the wound and normal skin appendages (like hair follicles and sweat duct glands) are still in place outside the wounded surface but they are damaged within the wound.

b) Tissue repair. A scab is formed covering the wounded surface and below it, keratinocytes start migrating from the cut edges, and from what remains of the skin appendages in the wounded area, to repair the epidermal layer. The main mechanism for this movement is lamellipodal crawling: the cells in the first rows extend lamellipodia that attach to extracellular matrix in the fibrin clot and tug the epithelium forward into the wounded area. Beneath, at the dermal level, activated fibroblast proliferate and give rise to the granulation tissue which actively contracts helping the advance of the wound edges.

c) Remodeling (a stage that can last more than an year) The wound area epithelium recovers progressively its original structure but dense and abnormally organized bundles of collagen remain at the dermal level. This makes the re-epithelialized area slightly higher than its surroundings. Healed skin will also not contain the usual skin appendages at the end.

In this work we will study embryonic epidermal wound healing taking as biological model the fruit fly Drosophila Melanogaster. In section 2 we present a simple mathematical model for epithelial sweeping in wild type fly embryos. We do a preliminary validation of this model using movies of laser wound healing of stage 14/15 fly embryos in section 2.2 and of Dorsal Closure (denoted DC) in section 3. Similar laser (and also mechanical) wounds have already been studied from a biochemical point of view in [11] where the authors modulated the activity of different small GTPases to evaluate their role in the way the wounds close.

There is no inflammation nor remodeling in the settings we will consider - it is regenerative repair in the sense defined in [2]. Note that regenerative healing does not imply that there is production of new cells - this is certainly not the case in DC and even if there can be some mitosis in embryo wound healing like the one we study, this is a marginal effect and happens away from the wound edge.

From a mechanical point of view, an essential feature of embryonic epidermal wound healing is that the main mechanism driving closure is acto-myosin cable contraction (also known as purse-string effect). This is a general behavior, not only for Drosophila [11], but also for other species like chick and mouse embryos - see [6] for a review.

As was shown in [11] (and is also clear in our own movies) in the few minutes that follow a laser (or a mechanical) wounding of the epidermis, filamentous actin and myosin II (a motor protein) are concentrated inside the adjacent cells (near the cytoskeletal membrane touching the wound). This gives rise to a local acto-myosin cable element. Such intercellular cable elements are anchored into adherens junctions between neighboring cells (which are locally reinforced for this purpose) and are thus all connected forming a supra-cellular acto-myosin cable that encircles the wounded area. This cable structure is continuously put under tension by the myosin molecular motors making the actin filaments slide relative to each other thus producing a global contraction effect that helps closing the epithelial wound (since this is a dynamic process the local cable tension does not necessarily decrease when the local cable element contracts). The position of this cable, at the boundary between the wound and the epidermis defines the Leading Edge (LE).

The actin cable also has the effect of organizing the advancing front (through a curvature flow type mechanism as we will describe below) and

restrain partially the formation and activity of filopodia produced by the LE cells. Although LE cells extend filopodia that actively sample the wound substratum ahead of them, in normal embryonic wounds they do not seem to exert significant traction forces during the advancement phase of re-epithelization. However, these filopodia are essential for the final adhesion phase where filopodial and lamellipodial structures play an important role in bringing together and knitting the wound edges that are within filopodial reach of each other.

The purse string mechanism is also important in adult wound healing (it was described as driving the closure of small wounds in adult mammalian cornea - the small size of the wound seems to be an important factor in this case) but, as we saw above, the main role in the adult setting is played by lamellipodial crawling. We remark that the vital importance of wound healing, led organisms to develop very robust mechanisms to make sure that it takes place. This involves having several redundant mechanisms available - this way, different mechanisms can be active simultaneously (or can be quickly activated) in the different settings, and take the place of the main one in case this one is perturbed. A striking example of this behavior is given in [11] where rho-mutant embryos do not have the capability of forming an actin cable around the wound but succeed in closing wounds by increasing the number and size of the filopodia at the LE - these filopodia from neighboring cells interact along the LE to contract it (the net effect being a new curvature dependent force term that draws the wound closed).

It is also interesting to note that there are settings where the wound closes by purse string in part of the boundary and by lamellipodial crawling in another like in monolayers of gut epithelial cells - see [5] figure 1. A remarkable feature of this image is that the convex part of the boundary closes by a purse-string mechanism while the concave part (which would open if its dynamics was governed by a curvature law) is closing by lamellipodial crawling - it is a good strategy for reducing the wound surface efficiently and right away.

Other interesting mathematical models (of a different nature) for epidermal wound healing have also been proposed (see [7] chapter 9 for a review). In future work we intend to consider mechanically more elaborate versions of our approach that take advantage of their point of view, but for this paper we will deliberately choose a simple mathematical formalism (based on the Laplacian for describing elasticity and curvature terms for describing actin cable contraction) and show that it already yields interesting results.

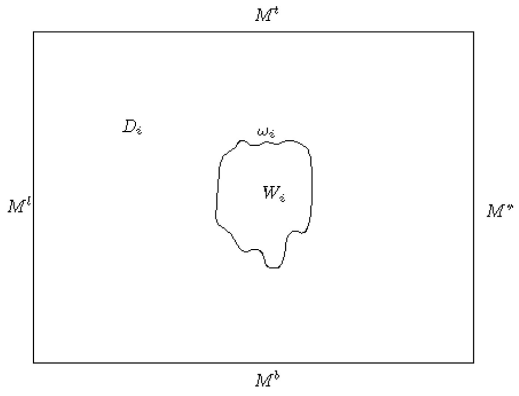

Figure 1: Computational domain.

2 Wound Healing

2.1 Simple Mathematical Model

We present here a simple model for simulating the movement of the boundary (LE) of an epidermal wound. For mathematical purposes, the LE will also be denoted by ω. Our simulation domain will be a rectangle, M, which contains our wound W (the part no longer occupied by the epidermis). The part of the domain occupied by the epidermis is $D = M \setminus W$. The wound W (and therefore also D) change in time. Actual mechanical behavior of the wound should at least obey nonlinear visco-elastic dynamics [7], but since epidermal wound closure occurs during a long time compared to the space scales involved, one may neglect inertial forces and consider the overall process as a succession of linear elastic equilibria, where we omit as well the successive initial stress fields. We will adopt such a so-called quasi-static approach to describe this evolution.

At each step $i = 1, \ldots, n$, W_i and D_i (see figure 1) denote the positions of the wound and the epidermis. We suppose the behavior of the epidermis to be elastic and subject to three forces:

1) epidermal tension (that pulls the wound open once the epidermis is cut) which we simulate by constant normal forces applied at the top (M^t) and bottom (M^b) boundaries of our simulation domain. The actual forces should be considerably more complicated and are due to the stress fields induced by the previous morphogenetic movements (as well as those occurring while the wound is healing). It is the epidermal tension that plays the main role in the initial opening of the wound but it also plays an important role during the wound closure (opposing the movement).

2) the actin cable tension. This term gives rise to a force that is proportional to the curvature at each point, in the spirit of what was described in [4] for the middle point of their arc of circle. Here, we extend this force to all the points on the LE - we work in a PDE framework instead of the ODE framework used in [4]. Supposing that the LE is parameterized in the positive (counter-clockwise) direction, this term will be described by a normal force which is proportional to the local curvature of the LE at each point. It points towards the exterior of D_i (i.e. towards the interior of the wound W_i) at the points of positive curvature and towards the its interior at points of negative curvature.

3) a uniform normal force pointing towards the exterior of D_i - this force is associated to the lamellipodial crawling or connective tissue contraction (as we saw above, in wounds the granulation tissue contracts to help the closure, the amnioserosa plays the same role in DC - see section 3).

The cytoskeleton and membrane of the cells of the epidermis are globally viewed as a mechanical continuum, which can bear traction and compression loads but not bending nor torsion. Assuming a linear elastic response of this medium considered as a plane surface, the elastic deformations are then in-plane. One obtains a simple continuum membrane model governed by a Poisson equation with suitable boundary conditions.

Moreover, the introduction of a Poisson model may also be considered as a quite acceptable approximation since in [3] (referring in particular to the seminal work [1]) it is indicated "Note, too, that many tissues exhibit a nearly incompressible behavior under physiologic loading, which is thought to arise from the high volume fraction of water in most soft tissues provided that the conditions of interest do not allow the water to diffuse into or out of the tissue during the period of interest." In such a framework, it is well known that when one takes into account the incompressibility, the general linear elasticity equations for homogeneous media reduce to a Poisson equation.

Therefore, at each time step i ,the corresponding displacement field u_i will satisfy

$$\begin{cases} -\Delta u_i = 0 \ \text{ in } \ D_i, \\ \dfrac{\partial u_i}{\partial n} = C_1 n \ \text{ on } M^t \cup M^b, \\ \dfrac{\partial u_i}{\partial n} = C_2 \kappa n + C_3 n \ \text{ on } \omega_i = \partial W_i, \\ u_i = v_i = \begin{pmatrix} C_4 \\ C_5 \end{pmatrix} \ \text{ on } M^l \cup M^r, \end{cases} \tag{1}$$

where n is the external unit normal to ∂D_i, κ is the curvature of ω_i and C_1, C_2, C_3 are constant parameters (in this simple model) which are determined using the experimental data. Since there seems to be an overall sliding movement of the epidermis that contains our wound (whose origin is not clearly identified and which we cannot model for the moment) we need to quotient the action of the translations on our system. This is done by supposing there is a series of translation vectors v_i (one for each step) such that $(u_i = v_i)$ on the left (M^l) and right (M^r) boundaries of the rectangular domain. We then optimize v_i at the same time as the other parameters of our problem to choose the appropriate translation at each step.

Once u_i is obtained, we consider its restriction the inner boundary ω_i (the leading edge) and displace this boundary (using a level set method) to obtain ω_{i+1}. The domain W_{i+1} enclosed by ω_{i+1} is the new position of the wound. More precisely, we compute the solution u_i of (1) on the domain D_i by using finite element methods on a triangular mesh. We obtain a vector field u_i, which is used as a velocity vector in the level set method in order to move ω_i.

The position of ω_{i+1} obtained also defines the new epidermal domain $D_{i+1} = M \setminus W_{i+1}$ which will be used in the following step to solve equation (1) in order to obtain u_{i+1}, and so on.

When examining our data consisting of time-lapse movies of laser wounds in the ventral area of stage 14 or 15 wild-type Drosophila embryos, we remark that there is a first phase, which we call opening phase, where the wound will start by opening under the action of the epidermal tension. As a matter of fact, the curvature term due to actin cable tension (which, according to [11], forms very quickly) is also active during this phase - it should help smoothening out the corners and making the wound more round. However, in the opening phase the pieces of cable seem to form locally and it is only later on, once they all connect and the cable is formed all around the wound, that it becomes globally efficient. We will consider modeling this phase in future works, in particular once we have more detailed data that allow us to describe this phenomenon - for the moment we have few images and it is difficult to determine the precise wound contour before the cable is formed

- the data we are able to gather are not significative enough for developing a reliable model.

In this paper we will thus concentrate on modeling the second phase, the closing of the wound. In this case, the main closing mechanism is actin cable contraction, the cable formation restrains filopodial and lamellipodial number and activity [11] and there is no evidence of the formation of a contractile connective tissue. Thus, we will optimize our parameters supposing $C_3 = 0$. This corresponds to keeping only the first two forces described, namely epidermal tension and actin cable contraction. However, the third force term will be of interest for the cases where the cable formation is inhibited or for adult wound healing where lamellipodial crawling plays the main role. We will also use it in the following section where we study dorsal closure.

For embryonic wound healing, in [11] they describe cases of mutants where the cable formation or the actin extensions (filopodia or lamellipodia) are perturbed and that, nevertheless, are able to accomplish (at least part of) the closure process. Even with this simple model, we can account for this type of behavior by supposing more complicated space and/or time variations of the parameters C_i (which will no longer be supposed to be constant but to vary in response to the up or down-regulation of the associated phenomena) and by adding a zipping coefficient C_6 as discussed in section 3.

We remark that we are doing all our analysis in 2D while the real dynamics is 3D. In fact, we try to obtain our original data keeping as much 3D information as possible (although the embryos are still flattened by their own weight - see section 4) and avoiding to interfere with the dynamics (in preceding works the embryos were squeezed between the coverslip and a permeable membrane which, although it has the advantage of reducing the spatial shifts, risks perturbing the movement and destroys the 3D character). However, for the moment, we project the confocal images to obtain 2D data which is simpler to treat (in particular for the contour extraction). Nevertheless, all the forces described in the model can be considered in 3D (in that case, one should naturally work on the tangent plane to the embryo at the point considered). This model also assumes a very simple mechanical behavior of the tissue since the precision of our present data (wounding precision, image acquisition and mechanical response of the tissues involved) do not justify more complicated assumptions. However, once the mechanical and 3D properties of the tissue can be determined in a more precise way, it will be interesting to include all relevant information in the model.

2.2 Numerical Simulation

As said in the previous section, we assume that the dynamics of the wound is governed by equations (1) where the magnitude of the parameters $(C_j)_{1\leq j\leq 5}$

are to be identified. Let $C = (C_1, C_2, C_3)$ the force coefficients, $C_T = (C_4, C_5)$ be the translation coefficients and $\tilde{C} = (C, C_T)$ be the set of all the parameters.

First, the offset (translation) coefficients C_T are computed *at each time step* i. To do so, experimental successive boundaries of the wound are computed by means of image processing/contour-extraction techniques. We consider at each time step i the experimentally observed boundary of the wound, ω_i^{EXP}, as initial boundary. For a given collection of parameters $\tilde{C}$, one solves the equations (1) in order to obtain a displacement u_i, which is used to evolve the initial boundary ω_i^{EXP} of the wound into an updated one ω_{i+1}^{PDE}.

For each i, let W_i^{EXP} and W_i^{PDE} denote the sets enclosed by ω_i^{EXP} and ω_i^{PDE}, respectively. The following observed boundary being ω_{i+1}^{EXP}, we consider the area of the set symmetric difference $W_{i+1}^{EXP} \ \Delta \ W_{i+1}^{PDE}$ as a quantification of the error to be minimized in order to obtain the correct values of the parameters $\tilde{C}$. The minimization of $|W_{i+1}^{EXP} \ \Delta \ W_{i+1}^{PDE}|$ (where $|\ |$ denotes the area of the set) yields the values of the components of $\tilde{C}$ at time step i and thus, in particular, that of the offset table C_T (these offsets are stored in order to be used in the second phase). Remarkably, we noticed that the mean-values of the byproduct components of the force coefficients C, namely $C_j(i)$ for $1 \leq j \leq 3$ turned out to be numerically close to the constant optimal values computed in phase two as explained next.

The aim of the second phase is to identify constant, time-independent force coefficients C which account for the overall model validation of wound closure. In other words, starting with initial wound $W_0^{PDE} = W_0^{EXP}$, we compare at each time-step $i \geq 1$ the experimentally observed wound W_i^{EXP} to the computed W_i^{PDE}, but unlike in the previous step, this time W_i^{PDE} is computed using the W_{i-1}^{PDE} as initial boundary.

The optimization problem amounts then to minimize the cost function J given by

$$J(C) = \sum_{i=1}^{m} |W_i^{EXP} \ \Delta \ W_i^{PDE}|$$

where m is the number of time evolutions considered in the optimization procedure (here we take $m = 9$, since we use 10 images) and for C we continue to use the optimized time-dependent offset C_T in equations (1) when computing $J(C)$.

Since the cost function J is non-smooth, classical gradient methods are useless. Moreover, one cannot exclude the existence of multiple local minima, for which descent methods are inefficient. To overcome these two drawbacks, we use a global optimization approach, based on the Genetic (`ga`) and Direct Search (`patternsearch`) modules provided by Matlab, by proceeding as follows: first, a genetic optimization is performed on the cost function J, with the aim of obtaining a final value of the parameter C close to the global optimum. Then, this first estimate is used as initial guess by the pattern

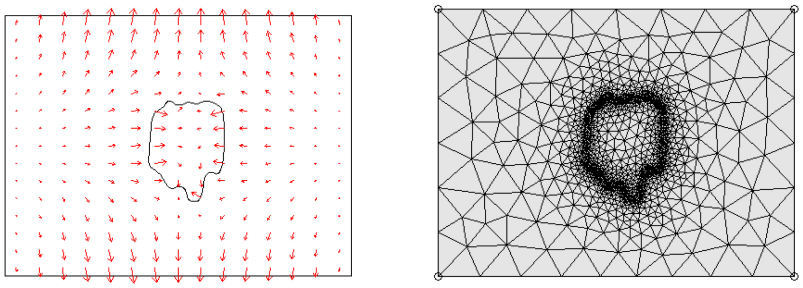

Figure 2: Example of a computed solution u_i with extension u_i^{int} (left) and the corresponding computational mesh (right).

search method in order to refine the optimum value of C.

A well known shortcoming of the above global minimizing algorithms is that they use extensive call to cost evaluation, which in our case amounts theoretically to solve, for each time step i, a large number of large scale linear systems (as many as the number of generations times the number of individuals per generation).

Fortunately, we can take advantage of the linearity of 1 to solve just one partial differential equation (PDE) for each significant parameter: for $j = 1, \ldots, 5$ and for each step $i = 0, \ldots, m-1$, we define $u_i^{j,1}$ to be the solution of problem 1 with $C_j = 1$ and $C_k = 0$ for $k \neq j$. The solution of 1 will be given by

$$u_i = \sum_{j=1}^{5} C_j u_i^{j,1} \ . \tag{2}$$

Moreover, since for wound healing we take $C_3 = 0$ and that the problem we obtain for the translation v_i (i.e. the parameters C_4 and C_5) has a constant solution (the same constant Dirichelet boundary conditions on the left and right sides of the rectangle and homogeneous Neumann elsewhere), we just have to compute $u_i^{1,1}$ and $u_i^{2,1}$. Once we have these solutions, u_i will just depend linearly on the parameters C_i which simplifies considerably the optimization of these parameters.

Having obtained u_i (see figure 2), to perform the evolution of our contour we use level set methods. The contour is implicitly represented as the zero level set of a function $\Phi(x)$ solution of a Hamilton-Jacobi equation. The main advantages of this approach is that the contours automatically merge and separate even in case there are changes of topology and that geometric quantities, such as normal vectors and curvature, are easy to calculate. The implicit representation of $\Phi(x)$ displaces all the level sets throughout the entire computational domain, not only the zero level set. Hence, we must be able to construct an extension velocity in the domain inside the inner boundary ω_i (i.e. in the wound W_i). This extension is in general not

straightforward and different approaches are proposed in the literature (see [10]). The main requirement for an extension velocity is that it smoothly approaches the prescribed interface velocity near the zero level set.

In our case the velocity field has a natural extension: the harmonic extension obtained solving

$$\begin{cases} -\Delta u_i^{int} = 0 \ \text{ in } \ W_i, \\ \\ u_i^{int} = u_i \ \text{ on } \omega_i. \end{cases} \tag{3}$$

Let U_i equal to u_i in D_i and u_i^{int} in W_i. We compute the new position ω_{i+1} of the wound as the zero level set of the function $\Phi_i(x)$, solution of the following Hamilton-Jacobi equation:

$$\partial_t \Phi_i(x,t) + U_i(x) \cdot \nabla \Phi_i(x,t) = 0. \tag{4}$$

The numerical simulations are performed in Matlab code (http://www.mathworks.com/) and by using Comsol Multiphysics software (http://www.comsol.com/) to compute the numerical solution of (1) and (3). We also used the toolbox of Ian M. Mitchell (http://www.cs.ubc.ca/~ mitchell) to implement level set methods.

The global optimization over the first 9 evolution steps (images 0 to 9) yields the coefficients $C_1 = 0.3891$ and $C_2 = 0.1493$. The simulated contours using these coefficients are shown in figure 3 (see also movie `Woundsimul.mov`) We give below the table of the quotients between the area of the symmetric difference $W_i^{EXP} \ \Delta \ W_i^{PDE}$ and the area of the computational domain M, or that of the open part of the wound W_i^{EXP}, at each time step (image) i. They are written as percentages. This table allows us to evaluate the relative errors committed (note that since $|W_i^{EXP}| \to 0$ at the end of the movie, it is not surprising to obtain high values for the final few images in the last row of the table).

Image Number	1	2	3	4	5	6	7	8	9
% with respect to domain size	0.4	0.4	0.6	0.5	0.3	0.4	0.1	0.2	0.1
% with respect to wound size	7.9	8.1	13.0	10.3	9.3	13.4	6.3	9.7	5.8
Image Number	10	11	12	13	14	15	16	17	18
% with respect to domain size	0.1	0.1	0.2	0.2	0.2	0.1	0.1	0.1	0.1
% with respect to wound size	9.0	8.1	12.3	15.8	18.3	10.9	25.3	36.6	135.7

The simulation is quite well validated by the final series of images (which, we recall, were not used for the optimization of the coefficients). This shows the pertinence of our model for simulating the closing phase of embryonic wound healing. In the last few images the real contour seems to close faster than the simulated one (which yields higher values of the quotients in the

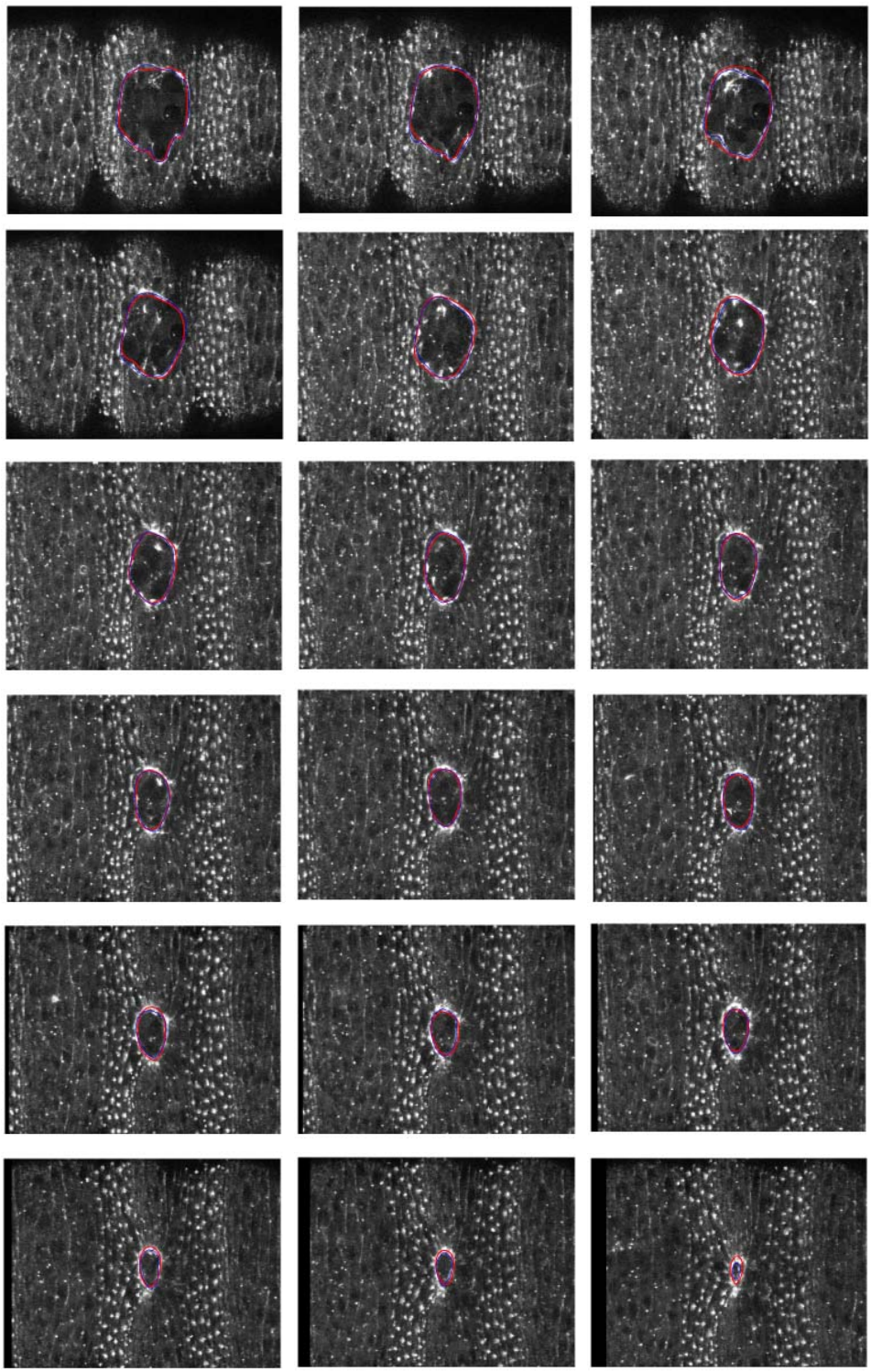

Figure 3: Wound images at successive times with extracted (blue) and simulated (red) contours. Time increases from left to right and top to bottom.

previous table). One possible explanation for this behavior is that, as mentioned in the introduction (see [11]) in this final phase the contribution of the filopodia and lamellipodia is no longer negligible. Therefore, our working assumption $C_3 = 0$ would no longer be verified. Taking $C_3 > 0$ in this final phase would yield a faster simulated closure and should thus allow us to follow the real contours better.

We remark that level set methods are also well adapted for doing curvature flows. Here we preferred the approach described above because in the spirit of [4] it is more natural to consider a curvature force resulting from the cable tension than an actual curvature flow of the boundary. The Laplacian also has the advantage of smoothening out the effect of strong forces concentrated in small areas of the boundary - this is an important advantage of this type of approach for dealing with the zipping in DC.

3 Dorsal Closure

This model of wound healing can be used for other kind of epithelial closure, such as Dorsal Closure (DC) in Drosophila. During embryogenesis, Drosophila embryos undergo epithelial folding and unfolding, which leads to a hole in the dorsal epidermis, transiently covered by a layer of large and thin cells called the amnioserosa (which, in DC, is the equivalent of the connective tissue - see figure 4). The cells in the dorsal-most row of the lateral epidermis are called the Leading Edge (LE) cells - these cells form the boundary of the lateral epidermis and they accumulate actin and myosin at their dorsal-most edge to form a contractile actomyosin cable just like we saw above for wound-healing (this cable is located at the boundary of the lateral epidermis and defines the LE). The hole is roughly shaped like an ellipse with major axis along the dorsal midline of the organism - which is along the anterior-posterior (AP) axis. By convention, we will always display our images with the anterior on the left, the posterior on the right and a horizontal AP axis. The anterior and posterior ends of the hole are called the canthi - the LE has a rather singular geometry at these points. The canthi separate the LE (also denoted ω_i for mathematical purposes, as in section 2) into two halves - the top margin, denoted ω_i^t, and the bottom margin, ω_i^b (in fact, in the original geometry of the embryo, these correspond to the right and left margins, respectively).

DC consists of the migration of lateral epidermal cells towards the midline covering this opening (the amnioserosa) in a couple of hours (see movie `DC.mov`). This process does not involve any cell division but only a coordinated reorganization and contraction of the actomyosin cytoskeleton in different populations of epithelial cells. As in wound healing, it implies the three following forces: 1) resistive tension from the stretched epidermis, 2) actin cable tension and 3) amnioserosa (connective tissue) contraction ([8]).

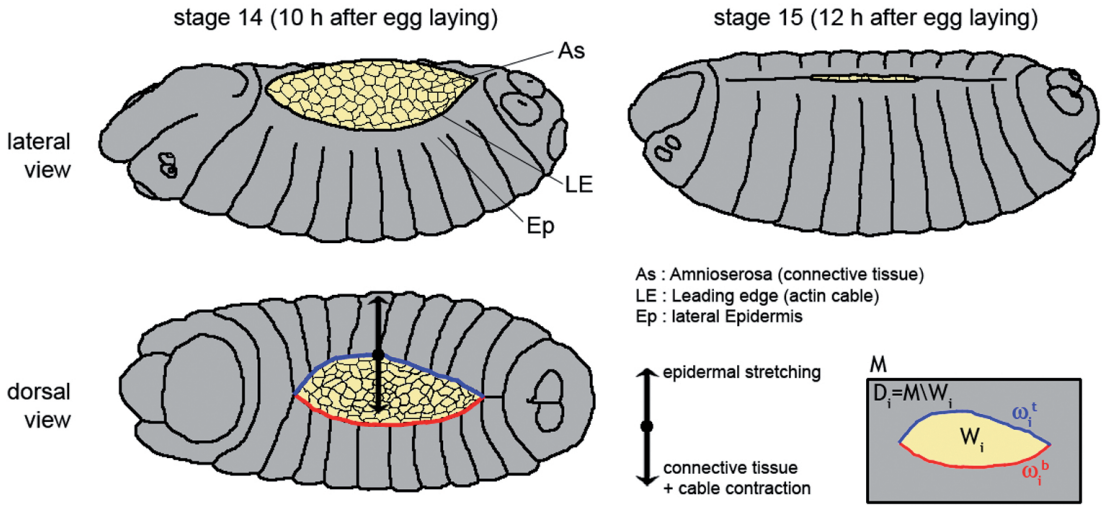

Figure 4: Scheme of tissues and forces implicated in dorsal closure in Drosophila embryos. The first row shows a dorso-lateral drawing of the drosophila embryo at stages 14 and 15. The second row shows a dorsal view of a stage 14 embryo and a representation of processes involved in the closure. Lines indicate the two tissues involved (the connective tissue of the amnioserosa consisting of thin and large polygonal epithelial cells in yellow, the epidermis consisting of columnar epithelial cells in gray) and in-between the Leading Edge (LE). We distinguish the top margin ω_i^t (in blue) and the bottom one ω_i^b (in red).

Moreover, the LE cells extend actin protrusions, filopodia, that intertwine near the canthi drawing towards each other and knitting the two margins - the canthi advance towards the middle of the opening a bit like zippers. This process (called zipping) is essential for the proper matching of cells along the anterior-posterior axis - as the two margins merge during dorsal closure the cells from each side of the epidermis that meet end up establishing permanent (adherens) junctions similar to those between the other epidermal cells. At the same time the actin corresponding to the cable segment they contained is de-polymerised and in the end there is no trace remaining of the fact that they were far apart at the outset of DC.

In DC zipping plays a very important role and has to be taken into account. This can also be the case for wound healing in situations where other main forces have been inhibited like the rho mutants described in [11]. In these settings a zipping term should be included in the model and the corresponding deformation (which we will denote u^6) should be added to the ones considered in the previous section.

In general, we can model the zipping force (Z) by a term of the type

$$Z(x) = \int_\omega f(x,y)\frac{y-x}{|y-x|}dy \quad \text{for all } x \in \omega \ , \tag{5}$$

where ω is the Leading Edge (LE). Unfortunately, our present experimental tools and data do not enable us to obtain enough information about the function f for precise modeling of its contribution. Nevertheless, we can assume that f depends on the distance between the points ($|x-y|$). Indeed, we can write, $f(x,y) = g(|x-y|)h(x,y)$, where the function $g : \mathbb{R}^+ \to \mathbb{R}$ has compact support inside $|x-y| < 2L$, where L is the maximum length of filopodia in the situation considered (it should depend on the particular fly line used).

This approach should also be appropriate for modeling the zipping in wound healing as long as the wound W (the set enclosed by the LE) is convex. If we deviate significantly from this setting, some caution is needed in particular concerning the ability of filopodia to pull cells when they establish contact outside W.

In DC, we have a particular geometry and behavior that simplifies the modeling of the zipping force. In the wild type setting (and most genetically modified settings we observed) there seems to be no zipping between points in the same margin, which implies that $f(x,y) = 0$ if x and y belong to the same margin (so, in practice, the integration in (5) is only over the opposite margin.

Moreover, the epidermis of the embryo is divided into 14 segments separated by sharp boundaries, each of them constituted by anterior and posterior cells (green and red cells, respectively, in movie `DC.mov`). This spatial organization is conserved at the end of DC by a proper segment adjustment

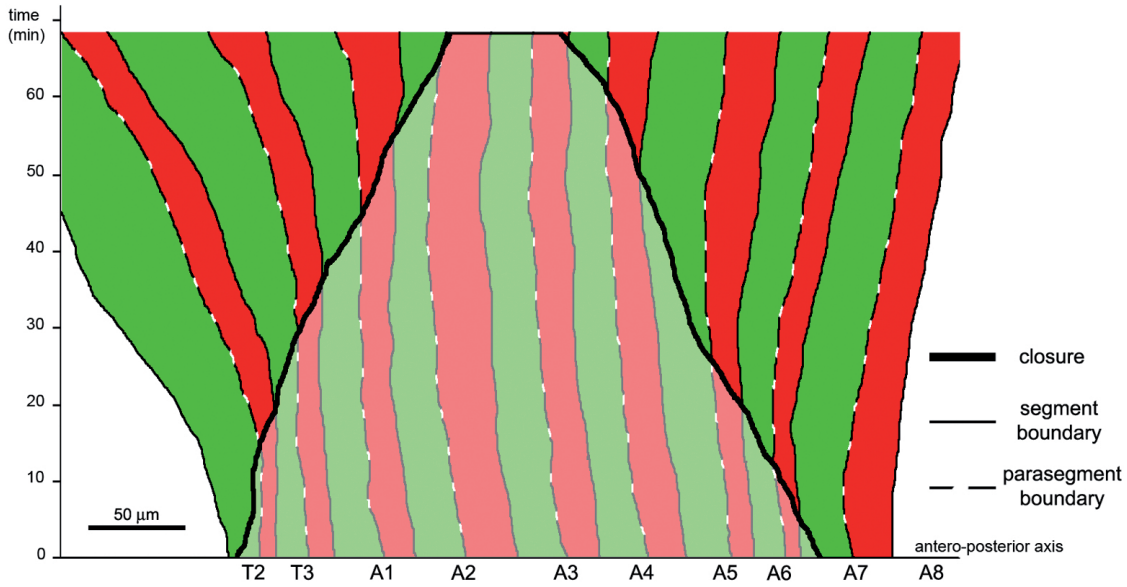

Figure 5: Antero-posterior stretching of segmental boundaries during dorsal closure. The central curve (bold line) shows the closure of each parasegmental and segmental boundaries during time, from a total opening (the "wound" goes from the segment T2 to the segment A7 at time 0') to the end of closure (the "wound" covers only parts of segments A2 and A3 at time 70'). The full and dashed lines show the shifts of segmental and parasegmental boundaries respectively. Curves have been obtained by tracking each boundary during dorsal closure of the embryo shown in movie `track.mov`. We can observe that anterior boundaries (from T2 to A2) begin to shift toward the anterior part of the organism only after each boundary is closed. This shift is due to the head involution but note that this later morphogenetic process does not disrupt the vertical movement of epidermal shifts prior to their fusion at the dorsal midline (the actin cable seems to isolate DC from the surrounding movements). Tail movement also gives rise to a similar but weaker shift after the closure of each posterior segment.

potentially mediated by filopodia ([9]). Tracking of segment and parasegment boundaries during DC indicates that physical points on the leading edge move vertically, i.e. orthogonally to the AP axis (figure 5).

If we want to take into account the fact that zipping plays a role in segment matching then f should also include specific information about the matching genes expressed by the cells present at points x and y. In the wild type context, in the beginning of DC the parasegments that should match are placed (considering our orientation convention of horizontal AP axis and symmetry relative to this axis) vertically to their counterparts in the opposite leading edge. Moreover, according to figure 5, they move approximatively vertically throughout DC. In this work, we will consider only cases where we have this symmetry, and simulate them by supposing that we have a vertical zipping force which is supported in the part of the leading edge where the vertical distance between the two margins is smaller than $2L$. To be precise, for each step i, we suppose that the upper leading edge (denoted ω_i^t) is described by a function $y = g_i(x)$ and the lower leading edge (denoted ω_i^b) by $y = h_i(x)$ for $x \in [c_a, c_p]$ where c_a and c_p are the x coordinates (horizontal positions) of the anterior and posterior canthi at step i. The zipping will then be effective only in the set $Z_i := \{(x, y) \in \omega_i \ : \ g_i(x) - h_i(x) \leq 2L\}$. We will consider more complex situations in the future.

In the spirit of section 2, at each step i the displacement field due to zipping u_i^6 will thus satisfy

$$\begin{cases} -\Delta u_i^6 = 0 \ \text{ in } \ D_i, \\ u_i^6 = 0 \ \text{ on } M^l \cup M^r, \\ \dfrac{\partial u_i^6}{\partial n} = 0 \ \text{ on } M^t \cup M^b, \\ \dfrac{\partial u_i^6}{\partial n} = 0 \ \text{ on } \omega_i \setminus Z_i, \\ \dfrac{\partial u_i^6}{\partial n} = \begin{pmatrix} 0 \\ -C_6 \end{pmatrix} \ \text{ on } \omega_i^t \cap Z_i, \\ \dfrac{\partial u_i^6}{\partial n} = \begin{pmatrix} 0 \\ C_6 \end{pmatrix} \ \text{ on } \omega_i^b \cap Z_i \ . \end{cases} \tag{6}$$

Thanks to linearity of the problem, the optimization is done by solving (6) with $C_6 = 1$ and then proceeding just as in the previous section. The global optimization yields the coefficients $C_1 = 0.5785$, $C_2 = 0.1677$, $C_3 = 0.6099$ and $C_6 = 0.5216$. The simulated contours using these coefficients are shown in figure 6 (see also movie `DCsimul.mov`). We also give below the table of the quotients between the area of the symmetric difference

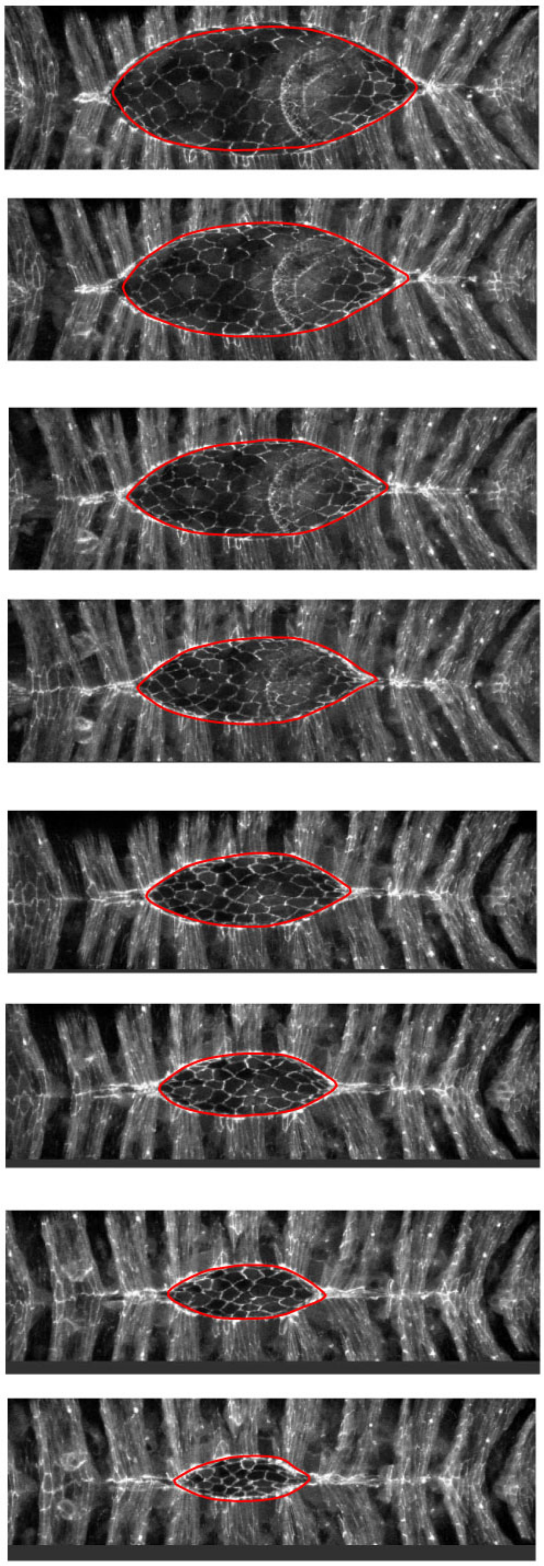

Figure 6: Dorsal Closure images at successive times with simulated contours (in red).

$W_i^{EXP} \Delta W_i^{PDE}$ and the area of the computational domain M, or that of the exposed amnioserosa W_i^{EXP}, at each time step (image) i. As before, it is given in percentage and allows us to evaluate the relative errors committed. (once more, $|W_i^{EXP}| \to 0$ at the end of the movie, yielding high values of the last row for the last few images).

N. Image	1	2	3	4	5	6	7	8	9
% with respect to domain	2.1	1.3	0.8	0.6	0.4	0.4	0.4	0.7	0.5
% with respect to amnioserosa	7.7	6.3	4.7	5.3	4.0	5.2	7.4	20.5	29.0

4 Appendix: Material and Methods

Genetics. The following fly lines were used: βcatenin-GFP (8556), UAS-h-actin-CFP (7064 from Bloomington Drosophila Stock Center), ptc-gal4 (gift from N. Perrimon), en-gal4 (gift from A. Brand), UAS-Dαcatenin-GFP and zipper-GFP (CC01226 from Flytrap Database). The following recombined lines or crosses were used for video time-lapse of dorsal closure or wound healing 1) w*; βcatenin-GFP, en-gal4 / UAS-h-actin-CFP 2) w*, ptc-gal4, UAS-Dαcatenin-GFP 3) zipper-GFP.

Live imaging and image treatment. Embryos are dechorionated in bleach then staged and placed dorsal side down on a coverslip. A coating of halocarbon oil, a piece of damp paper and a hermetic chamber ensure hydration (and normal development of 95% of embryos into larvae in control experiments). Embryos are neither fixed or pressed, nor glued, to ensure that dynamics are not modified by any external force. They naturally lay on their dorsal part when put in the viscous oil, which is convenient to film dorsal closure. In order to film wound healing on the lateral or ventral parts of embryos, the embryo of interest is stuck between two embryos lying on their dorsal part. This method is sufficient to immobilize the external part of the organism but movements are still possible inside the vitelline membrane (the membrane is a protective layer outside the epidermis, layer from which the larvae hatches after embryogenesis). Unless embryos are completely pressed (which risks modifying significantly closure dynamics), these sliding movements inside the vitelline membrane are unavoidable and force us to quotient out translations in order to follow wound closures. Images are taken with a Zeiss LSM 510 Meta confocal inverted microscope using x40 1.3 NA oil immersion objectives. Films last from 2 to 5 hours with stacks of 25 images (thickness from 30 to 40 μm) every 5 minutes. We assemble images and movies using ImageJ. Stacks are projected using a maximal intensity projection.

Laser ablations. Wounds are made using a Spectraphysics Tsunami pulsed biphoton laser blocked at 800 nm and using the "bleach control" software of

Zeiss. Images are taken with a confocal system similar to the one described above.

5 Movie Captions

dorsal-closure.mov: Confocal time-lapse images taken from an embryo showing in green an ubiquitous membrane marker βcatenin-GFP and in red the posterior compartments with actin-CFP (Genotype: βcatenin-GFP ; en-Gal4, UAS-actin-CFP).
track.mov: Confocal time-lapse images taken from an embryo showing in gray a membrane marker only in the anterior compartments. Parasegmental and segmental boundaries can thus be tracked during the closure. Note that some cells in posterior compartments (see arrowheads on the first image) are marked too but the segmental boundary lies just posteriorly to these cells. (Genotype: ptc-gal4, UAS-Dαcatenin-GFP).
DCsimul.mov: dorsal closure images taken from the movie PtcCat.mov at successive times with simulated contours (in red).
Woundsimul.mov: confocal time lapse images taken from a wounded embryo with extracted (blue) and simulated (red) contours (Genotype: zipper-GFP).

References

[1] Fung, Y.C., *Biomechanics: Mechanical Properties of Living Tissues*, second ed. Springer, New York, 1993.

[2] Gurtner, G.; Werner, S.; Barrandon, Y. and Longaker M., *Wound repair and regeneration*, Nature, 453, pp. 314-321, 2008.

[3] Humphrey, J.D., *Continuum biomechanics of soft biological tissues*, Proc. R. Soc. A 459, pp. 346, 2003.

[4] Hutson, M. S.; Tokutake, Y.; Chang, M. S.; Bloor, J. W.; Venakides, S.; Kiehart, D. P. and Edwards, G. S. *Forces for morphogenesis investigated with laser microsurgery and quantitative modeling*, Science 300, pp. 145-149, 2003.

[5] Jacinto, A.; Martinez-Arias, A. and Martin, P., *Wound repair and regeneration*, Nat. Cell Bio., 3, pp. 117-123, 2001.

[6] Martin, P. and Parkhurst, S. *Parallels between tissue repair and embryo morphogenesis* Development, 131, pp. 3021-3034, 2004

[7] Murray, J.D. *Mathematical Biology*, vol. 2, Springer-Verlag, 2003.

[8] Kiehart, D. P.; Galbraith, C. G.; Edwards, K. A.; Rickoll, W. L. and Montague, R. A. *Multiple forces contribute to cell sheet morphogenesis for dorsal closure in Drosophila*, J. Cell Biol., 149, pp. 471-490, 2000.

[9] Millard, T.; Martin, P., *Dynamic analysis of filopodial interactions during the zippering phase of Drosophila dorsal closure*, Development, 135, pp. 621-626, 2008.

[10] Sethian, J.A. and Smereka P., *Level Set Methods for Fluid Interfaces*, Annual Review of Fluid Mechanics, 35, pp.341-372, 2003.

[11] Wood, W.; Jacinto, A.; Grose, R.; Woolner, S.; Gale, J.; Wilson, C. and Martin, P., *Wound healing recapitulates morphogenesis in Drosophila embryos*, Nat. Cell Biol., 4, pp. 907-912, 2002.